

# Knowledge-Driven Learning via Experts Consult for Thyroid Nodule Classification

Danilo Avola<sup>1</sup>, Luigi Cinque<sup>1</sup>, Alessio Fagioli<sup>1</sup>,  
 Sebastiano Filetti<sup>2</sup>, Giorgio Grani<sup>2</sup>, and Emanuele Rodol<sup>1</sup>

<sup>1</sup> Department of Computer Science, Sapienza University,  
 Via Salaria 113, Rome, Italy

{avola,cinque,fagioli,rodol}@di.uniroma1.it

<sup>2</sup> Department of Translational and Precision Medicine, Policlinico Umberto I,  
 Viale del Policlinico 155, Rome, Italy  
 {sebastiano.filetti,giorgio.grani}@uniroma1.it

**Abstract.** Computer-aided diagnosis (CAD) is becoming a prominent approach to assist clinicians spanning across multiple fields. These automated systems take advantage of various computer vision (CV) procedures, as well as artificial intelligence (AI) techniques, so that a diagnosis of a given image (e.g., computed tomography and ultrasound) can be formulated. Advances in both areas (CV and AI) are enabling ever increasing performances of CAD systems, which can ultimately avoid performing invasive procedures such as fine-needle aspiration. In this study, we focus on thyroid ultrasonography to present a novel knowledge-driven classification framework. The proposed system leverages cues provided by an ensemble of experts, in order to guide the learning phase of a Densely Connected Convolutional Network (DenseNet). The ensemble is composed by various networks pretrained on ImageNet, including AlexNet, ResNet, VGG, and others, so that previously computed feature parameters could be used to create ultrasonography domain experts via transfer learning, decreasing, moreover, the number of samples required for training. To validate the proposed method, extensive experiments were performed, providing detailed performances for both the experts ensemble and the knowledge-driven DenseNet. The obtained results, show how the the proposed system can become a great asset when formulating a diagnosis, by leveraging previous knowledge derived from a consult.

**Keywords:** Image classification · Deep learning · Transfer learning

## 1 Introduction

Thyroid nodules, described by an abnormal growth of the gland tissue, are a common disease affecting the thyroid gland [12]. Ultrasonography is the most used modality to both detect and diagnose nodules. This method is safe, convenient, non-invasive, and has a better capability of distinguishing benign nodules from malignant ones, with respect to other techniques such as computed tomography (CT) and magnetic resonance imaging (MRI), facilitating early diagnosis

and treatment choice [17]. In order to take full advantage of ultrasound images (US), computer-aided diagnosis (CAD) is rapidly evolving, resulting in systems able to provide less subjective interpretations and, consequently, more precise diagnoses. A CAD system is generally developed following established phases including image preprocessing (e.g., noise removal, image reconstruction, etc.), region-of-interest (ROI) extraction, segmentation, and classification. Historically, many of the available works focus on the first three steps, while in the latest years the emphasis is being shifted towards thyroid nodule classification due to the evolution of machine learning approaches. A key aspect of all phases lies in the nodule representation, where techniques such as local patterns (e.g., LDP and LBP [25]), or wavelet transform (e.g., DWT [18]), can provide a detailed description of the gland itself. By applying these techniques, as well as a plethora of other computer vision approaches, it is ultimately becoming possible to detect and segment the thyroid inside a US image [3,27], as well as classify nodules [13], thus making CAD a great asset for clinicians during their diagnoses.

### 1.1 Related work

In the latest years, many interesting works using various machine learning approaches concerning the nodule classification task, were presented. In [22], a comparison between Bayesian techniques, Support Vector Machines, and Neural Networks, shows promising results for the latter, close to classic radiological methods. By using the EM algorithm to train a CNN, a network able to grasp correlations in an image through convolutions, the authors of [21] can further improve performances of an automatic system trained in a semi-supervised way. While convolutional networks are certainly powerful, representing the nodules in a meaningful way can give an edge on the diagnosis accuracy, especially when few samples are available. In [11], HOG and LBP features are successfully combined with other high-level features, in order to compensate the lack of thyroid images. Another approach to solve the issue of small datasets, common problem for medical researches, is data augmentation. For this procedure, traditional methods include image cropping, rotation, and scaling, although even neural networks, such as GANs, can be used to increase the dataset size. Indeed, in [28] data augmentation is performed through CNNs, in order to achieve improved performances with respect to standard US. A different approach to handle small-sized datasets, is transfer learning. Through this method, a network trained on a different task is reused to reach convergence faster and more easily on the new domain. The authors of [15] exploit this technique in combination with a feature fusion procedure, where US images of thyroid glands are fused together with their respective elasticity maps, ultimately exceeding state-of-the-art performances.

While much was done concerning the classification through neural networks and transfer learning, other approaches are also emerging based on either ensemble learning or domain knowledge transfer. In [9], by using an ensemble, the authors are able to exceed radiologists performances for thyroid nodule classification. Other works successfully applying and, thus, encouraging the use of the ensemble technique are [5] and [24]. The former is able to perform white matter

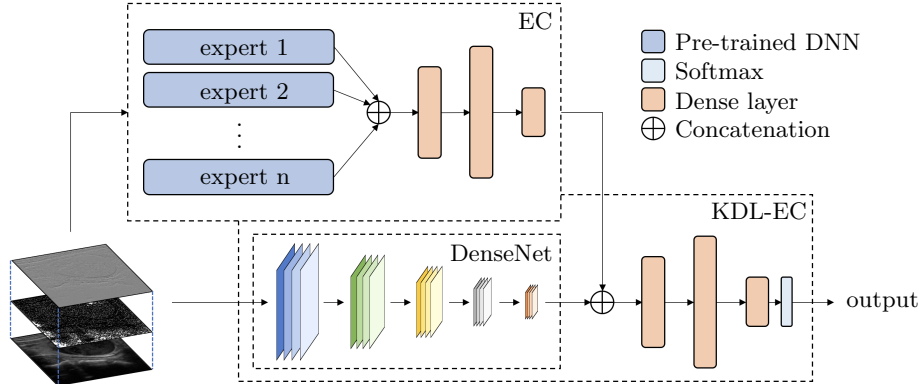


**Fig. 1.** Knowledge-driven learning (KDL) via experts consult (EC) framework architecture. The feature fusion between US, LBP and DWT images is given as input to the EC module and to the KDL-EC DenseNet. Their outputs are then concatenated and elaborated by dense layers to obtain a diagnosis. The EC module, through an ensemble of deep neural networks (DNN), can drive the KDL-EC unit learning.

fiber clustering, while the latter can classify lung nodules from CT scans with high accuracy. Concerning the domain knowledge transfer, in [1], from which we have taken inspiration for this study, the authors effectively drive the learning using prior knowledge of a different network. In [10], the authors apply a similar knowledge-driven rationale to diagnose breast cancer by integrating domain knowledge during the training phase, ultimately showing that this approach can be used to formulate a medical diagnosis.

In this study, due to the relatively small dataset at our disposal, we applied both data augmentation and feature fusion in order to fully exploit the available images. Moreover, we decided to explore knowledge-driven approaches using an ensemble of experts obtained via transfer learning. The ensemble guides a DenseNet during its training by providing consults, and both components finally collaborate to act as a CAD system. Experimental results suggest that, while transfer learning is a powerful technique to handle smaller datasets, by leveraging prior knowledge through the experts ensemble consult, it is possible to drive the learning phase, thus training a good performing classifier for thyroid nodule computer-aided diagnosis.

## 2 Method

The proposed knowledge-driven learning via experts consult framework, shown in Figure 1, can be divided into three components: a data augmentation and feature fusion phase, where detail-rich nodule images are generated; an expert consult (EC) module based on the ensemble stacking technique, where pre-trained deep neural networks are fine-tuned; and a knowledge-driven learning (KDL) unit, where cues are given to a convolutional network during its training.

The first augmentation and fusion component is a mandatory choice for the proposed framework, due to the used dataset being relatively small. Data augmentation is performed computing LBP and DWT images for each US thyroid nodule. Feature fusion is then obtained by stacking the nodule US with its corresponding LBP and DWT images, along their channels axis. Since all images are grayscale, this procedure results in an object representing a nodule with shape  $(w * h * 3)$ , where  $w$  and  $h$  correspond to width and height of the image; while each channel is a different representation of the nodule. LBP and DWT representations were chosen since they provide further information about both inner and outer properties of the nodule itself, as shown in Figure 2. Finally, the feature fusion object is used as input for the other two components.

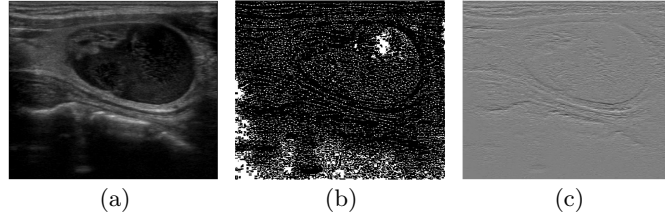


**Fig. 2.** Data augmented nodule example. In (a), the raw US image, while (b) and (c) show the same nodule analysed via LBP and DWT, respectively.

In the second component, an ensemble stacking module is fine-tuned in order to later help training another network. The ensemble is composed by  $n$  pre-trained deep neural networks, defined experts in this work, taking as input the described feature fusion object, which is normalized via a convolutional layer to handle the different representations. Each expert is first fine-tuned on the thyroid dataset and then used to build the ensemble, so that all members can operate simultaneously to formulate a diagnosis. To obtain a stacking ensemble, predictions of all  $n$  experts are concatenated and re-elaborated through 3 dense layers, so that the opinion (i.e., prediction) of each expert is taken into account for the final diagnosis. During this re-elaboration phase, all the experts are left untouched. As experts, several good performing networks pre-trained on ImageNet [4] were used, namely: AlexNet [8], DenseNet [7], GoogleNet [20], ResNet [6], ResNeXt [23], and VGG [19]. These pre-trained networks allow to apply the transfer learning technique, where previous knowledge is transferred and used on a new domain. Notice that while the chosen models are trained on non-medical images, some common characteristics, such as object contours, are still present in the new domain and can be effectively used on the new task, as already shown by the authors of [15]. Through transfer learning, it is possible to reduce both time and number of samples required to fully train a network, thus making this technique ideal for the proposed ensemble which is based on hard-to-come-by medical images. Finally, once the ensemble stacking module is trained on the

thyroid images, its diagnoses are used to provide a medical consult and drive the learning of the last module of the proposed framework.

The third and last framework component, is the knowledge-driven learning (KDL) unit. In this module, a convolutional neural network is given cues to help it achieve better performances on its classification task. The convolutional network of choice for this study is a DenseNet that, due to dense connections between convolutions, is able to forward propagate relevant information, thus obtaining interesting results on diverse tasks analysing both medical [16] and non-medical images [2,26]. Similarly to the ensemble module, the KDL-EC unit receives as input a feature fusion object, normalized via a convolutional layer to handle the different representations, to fine-tune the ImageNet pre-trained DenseNet. The output is then concatenated to the ensemble stacking prediction and re-elaborated with three dense layers, ultimately obtaining a diagnosis prediction through a softmax function. Notice that the expert consult is effectively guiding the learning of the DenseNet because the loss function is computed after the re-elaboration, and back-propagated all the way through the DenseNet itself while the experts ensemble remains left untouched.

### 3 Experimental Results

In this section, the private dataset and the hardware configuration used to test the proposed framework are first introduced, the experimental results for all the mentioned components are then presented.

#### 3.1 Dataset and Hardware Configuration

All the experimental results shown in this section are carried out on a private dataset of thyroid nodules, provided by the hospital Policlinico Umberto I of Rome. The dataset, collected from 230 distinct patients, is composed by 678 unmarked grayscale ultrasound images generated directly from the DICOM format, and cropped to a size of  $440 \times 440$  so that the thyroid gland is retained. Moreover, each image has a TI-RADS classification associated, utilised to split the available samples into the benign and malignant categories. All images with a score  $\leq 2$  are labelled as the former, while the remaining samples (i.e., with a score  $\geq 3$ ) are associated to the latter, thus defining a binary classification task. Examples of benign and malignant nodules, are shown in Figure 3. After this nodule-label association, the dataset was split into two sets,  $D1$  and  $D2$ , with non overlapping patients.  $D1$  contains 452 samples, divided into 360 benign and 92 malignant cases while  $D2$  comprises 226 images, partitioned into 180 benign and 46 malignant cases. This subdivision enables us to obtain unbiased results for both the EC and KLD-EC modules during their experimentation, since they are trained on different datasets. Concerning the hardware configuration, all tests are performed on the Google Cloud Platform (GCP), leveraging the pytorch framework and using a Virtual Machine with the following specifications: 4-Core Intel i7 2.60GHz CPU with 16GB of RAM, and a Tesla P100 GPU.

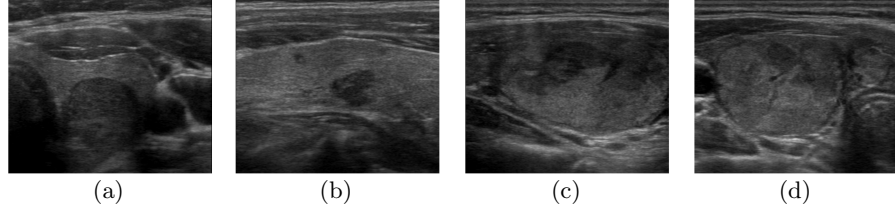


**Fig. 3.** Images from the utilised thyroid dataset. Benign examples are shown in (a) and (b), while malignant nodules are represented in (c) and (d).

### 3.2 Results

In order to fully assess the proposed KDL-EC framework, a preliminary grid-search is employed to evaluate various ImageNet pre-trained networks. The networks of choice are: AlexNet, DenseNet, GoogleNet, ResNet, ResNeXt, and VGG. Each network is available with pre-trained weights in the torchvision library of the pytorch framework. For each model, the best ImageNet performing version is selected, following the scores reported in [14]. All networks were trained for 1000 epochs, using a learning rate of 0.001, a batch size of 32, and  $[0.2, 1]$  as class weights to handle the discrepancy in the number of samples between the benign and malignant classes, respectively. Relevant results on the  $D1$  dataset, comparing 10 cross-validation performances with non overlapping patients on raw US images, augmented (i.e., US, LBP, and DWT) and feature fusion datasets, are summarized in Table 1. As shown, using either the augmented or feature fusion datasets, results in consistently improved performances. The rationale behind this behaviour can be attributed to the extra information both the LBP and DWT can provide, in the augmented dataset, and the ability to directly correlate visual cues among the various representations, in the feature fusion dataset. Moreover, as also shown by the authors of [15], by maintaining previously computed weights via frozen layers, it is possible to achieve conspicuous performances boosts through the transfer learning and network fine-tuning techniques. Indeed, as shown in Table 1, the best results for all networks are obtained by using both the feature fusion dataset and by freezing either 25% or 50% layers of the corresponding ImageNet pre-trained network.

Concerning the experts consult unit performances, the best performing networks are chosen to create an ensemble for the EC module according to the preliminary grid-search results. The EC members are selected in decreasing performances order. All tests are conducted on the feature fusion dataset  $D1$ , using an EC module of size 3, 5, and 7, employing a non-overlapping 10 cross-validation approach. In the EC-7, two different implementations of a DenseNet (i.e., DenseNet169 and DenseNet201 from [14]) are used to build the ensemble. This decision is taken due to the DenseNet obtaining the best performance on the feature fusion dataset. In Table 2, common evaluation metrics for a baseline network and the three EC models, are summarized. As shown, increasing the number of experts, allows the module to obtain better overall performances, even

**Table 1.** Average 10-cross validation models accuracies of baseline pre-trained models and various percentages of frozen layers. In each configuration block, accuracies on raw US, augmented (i.e., US, LBP and DWT) and feature fusion datasets (i.e., left, center, and right column of each block, respectively), are shown.

| Model     | Baseline% |      |      | Frozen-25% |      |             | Frozen-50% |      |             | Frozen-75% |      |      |
|-----------|-----------|------|------|------------|------|-------------|------------|------|-------------|------------|------|------|
| AlexNet   | 70.2      | 71.4 | 74.2 | 75.5       | 76.7 | 78.1        | 79.9       | 82.0 | <b>83.1</b> | 73.8       | 74.0 | 74.8 |
| DenseNet  | 76.8      | 78.0 | 81.5 | 80.6       | 82.8 | <b>87.2</b> | 78.3       | 79.6 | 83.4        | 77.4       | 78.5 | 82.0 |
| GoogleNet | 71.8      | 73.2 | 76.9 | 80.0       | 82.3 | <b>84.9</b> | 74.9       | 77.8 | 81.6        | 72.0       | 76.5 | 79.3 |
| ResNet    | 74.5      | 75.3 | 77.4 | 76.5       | 79.3 | 81.2        | 78.7       | 81.2 | <b>84.6</b> | 75.7       | 76.7 | 78.7 |
| ResNeXt   | 73.8      | 74.3 | 77.9 | 76.7       | 80.5 | 82.5        | 82.0       | 83.1 | <b>84.7</b> | 76.2       | 77.5 | 80.7 |
| VGG       | 75.6      | 76.4 | 80.3 | 77.3       | 81.5 | 83.1        | 81.2       | 83.4 | <b>85.6</b> | 76.8       | 78.9 | 81.6 |

though the single networks cannot perform as well as the EC module. The rationale behind this behaviour can be attributed to the ensemble stacking technique, where the outputs of the single networks (i.e., the experts) are re-elaborated in order to produce a better representation of the input and, consequently, a more accurate output. Notice that specificity scores are slightly lower than sensitivity ones, due to the dataset being skewed toward the benign class, even though class weights are utilised to represent the difference in the number of samples.

**Table 2.** Average 10-cross validation performances for the ensemble consult module (EC) at different sizes. The baseline scores refer to the best performing network: a feature fusion fine-tuned DenseNet. Scores are computed on dataset *D1*.

| Model    | Accuracy%        | Sensitivity%     | Specificity%     | AUC%             |
|----------|------------------|------------------|------------------|------------------|
| Baseline | $87.20 \pm 0.77$ | $87.50 \pm 1.13$ | $83.33 \pm 1.17$ | $89.12 \pm 1.45$ |
| EC-3     | $89.36 \pm 0.93$ | $89.61 \pm 0.92$ | $84.95 \pm 0.77$ | $91.33 \pm 1.11$ |
| EC-5     | $90.09 \pm 0.68$ | $90.37 \pm 0.85$ | $85.39 \pm 1.02$ | $92.78 \pm 1.09$ |
| EC-7     | $91.25 \pm 0.71$ | $91.94 \pm 0.73$ | $86.22 \pm 0.59$ | $93.06 \pm 1.34$ |

In relation to the KDL-EC unit performances, all experiments are carried out on dataset *D2*, in order to obtain unbiased results. Similarly to the EC module, a non-overlapping 10 cross-validation approach is used to evaluate this component. Moreover, the KDL-EC unit is tested using three different experts consults composed by 3, 5, and 7 members. The ensemble networks are the same used for the EC module and remain frozen during the training phase of the KDL-EC unit. The base network of choice for the KDL-EC is a DenseNet, selected due to obtaining the best scores in the preliminary results. The DenseNet is trained for 1000 epochs, a learning rate of 0.001, a batch size of 32, and uses class weights set to [0.2, 1] for benign and malignant samples, respectively. In Table 3, common evaluation metrics for a baseline network and the three KDL-EC models, are compared. As shown, adding cues based on previous knowledge during the learning phase (i.e., experts consult output), can drastically increase the performance of the DenseNet. Even more interesting, is the increase in the

specificity score, which is related to the malignant samples. In this case, even though the dataset is skewed toward the benign class, the network is still able to increase its performance by leveraging the EC model output.

**Table 3.** Average 10-cross validation performances for the knowledge-driven learning via experts consult module (KDL-EC) at different sizes. The baseline scores refer to the best performing EC module. Scores are computed on dataset *D2*.

| Model    | Accuracy%        | Sensitivity%     | Specificity%     | AUC%             |
|----------|------------------|------------------|------------------|------------------|
| Baseline | 91.07 $\pm$ 1.04 | 91.47 $\pm$ 1.17 | 90.09 $\pm$ 1.33 | 94.02 $\pm$ 1.27 |
| KDL-EC-3 | 94.83 $\pm$ 0.83 | 95.78 $\pm$ 1.12 | 92.22 $\pm$ 1.13 | 97.75 $\pm$ 1.10 |
| KDL-EC-5 | 94.95 $\pm$ 0.94 | 95.94 $\pm$ 1.03 | 92.67 $\pm$ 0.99 | 97.97 $\pm$ 1.12 |
| KDL-EC-7 | 95.11 $\pm$ 0.99 | 96.22 $\pm$ 1.23 | 93.09 $\pm$ 1.38 | 98.79 $\pm$ 0.93 |

Finally, in Table 4, a comparison with other relevant works, is presented. Although each method is tested on a different dataset, the reported results still allow to assess the performances of the proposed framework. As shown, the KDL-EC framework, thanks to its feature fusion and knowledge-driven learning approach, is able to achieve significant performances.

**Table 4.** State-of-the-art methods performances comparison.

| Method           | Accuracy%    | Sensitivity% | Specificity% | AUC%         |
|------------------|--------------|--------------|--------------|--------------|
| Wu et al. [22]   | 84.74        | 92.31        | 76.00        | 91.03        |
| Li et al. [9]    | 89.80        | 93.40        | 86.10        | 94.70        |
| Wang et al. [21] | 88.25        | 90.00        | 86.50        | 92.86        |
| Liu et al. [11]  | 93.10        | 90.80        | 94.50        | 97.70        |
| Zhu et al. [28]  | 93.75        | 93.96        | 92.68        | -            |
| Qin et al. [15]  | 94.70        | 92.77        | <b>97.96</b> | 98.77        |
| <b>KDL-EC</b>    | <b>95.11</b> | <b>96.22</b> | 93.09        | <b>98.79</b> |

## 4 Conclusion

In this paper, a knowledge-driven learning via experts consult framework for thyroid nodule classification is presented. As shown, by leveraging previous knowledge obtained by an ensemble of experts (i.e., a consult), it is possible to guide a new network during its training phase, and ultimately obtain improved results with respect to both the base network as well as the ensemble itself. As future work, more images are going to be collected and possibly released, so that a common ground for other works can be established. Moreover, further experiments on the proposed knowledge-driven approach utilising different types of input (e.g., elasticity maps), as well as a complementary module handling the TI-RADS classification in an automatic fashion, will also be considered.

## References

1. Avola, D., Cascio, M., Cinque, L., Fagioli, A., Foresti, G.L., Massaroni, C.: Master and rookie networks for person re-identification. In: International Conference on Computer Analysis of Images and Patterns. pp. 470–479 (2019)
2. Avola, D., Cascio, M., Cinque, L., Foresti, G.L., Massaroni, C., Rodolà, E.: 2d skeleton-based action recognition via two-branch stacked lstm-rnns. *IEEE Transactions on Multimedia* **9999**, 1–1 (2019)
3. Chang, C.Y., Lei, Y.F., Tseng, C.H., Shih, S.R.: Thyroid segmentation and volume estimation in ultrasound images. *IEEE transactions on biomedical engineering* **57**(6), 1348–1357 (2010)
4. Deng, J., Dong, W., Socher, R., Li, L.J., Li, K., Fei-Fei, L.: Imagenet: A large-scale hierarchical image database. In: 2009 IEEE conference on computer vision and pattern recognition. pp. 248–255 (2009)
5. Gupta, V., Thomopoulos, S.I., Rashid, F.M., Thompson, P.M.: Fibernet: An ensemble deep learning framework for clustering white matter fibers. In: International Conference on Medical Image Computing and Computer-Assisted Intervention. pp. 548–555 (2017)
6. He, K., Zhang, X., Ren, S., Sun, J.: Deep residual learning for image recognition. In: Proceedings of the IEEE conference on computer vision and pattern recognition. pp. 770–778 (2016)
7. Huang, G., Liu, Z., Van Der Maaten, L., Weinberger, K.Q.: Densely connected convolutional networks. In: Proceedings of the IEEE conference on computer vision and pattern recognition. pp. 4700–4708 (2017)
8. Krizhevsky, A., Sutskever, I., Hinton, G.E.: Imagenet classification with deep convolutional neural networks. In: Advances in neural information processing systems. pp. 1097–1105 (2012)
9. Li, X., Zhang, S., Zhang, Q., Wei, X., Pan, Y., Zhao, J., Xin, X., Qin, C., Wang, X., Li, J., et al.: Diagnosis of thyroid cancer using deep convolutional neural network models applied to sonographic images: a retrospective, multicohort, diagnostic study. *The Lancet Oncology* **20**(2), 193–201 (2019)
10. Liu, J., Li, W., Zhao, N., Cao, K., Yin, Y., Song, Q., Chen, H., Gong, X.: Integrate domain knowledge in training cnn for ultrasonography breast cancer diagnosis. In: International Conference on Medical Image Computing and Computer-Assisted Intervention. pp. 868–875 (2018)
11. Liu, T., Xie, S., Yu, J., Niu, L., Sun, W.: Classification of thyroid nodules in ultrasound images using deep model based transfer learning and hybrid features. In: 2017 IEEE International Conference on Acoustics, Speech and Signal Processing (ICASSP). pp. 919–923 (2017)
12. Moon, W.J., Baek, J.H., Jung, S.L., Kim, D.W., Kim, E.K., Kim, J.Y., Kwak, J.Y., Lee, J.H., Lee, J.H., Lee, Y.H., et al.: Ultrasonography and the ultrasound-based management of thyroid nodules: consensus statement and recommendations. *Korean journal of radiology* **12**(1), 1–14 (2011)
13. Persichetti, A., Di Stasio, E., Guglielmi, R., Bizzarri, G., Taccogna, S., Misischi, I., Graziano, F., Petrucci, L., Bianchini, A., Papini, E.: Predictive value of malignancy of thyroid nodule ultrasound classification systems: a prospective study. *The Journal of Clinical Endocrinology & Metabolism* **103**(4), 1359–1368 (2018)
14. Pytorch: torchvision network models. <https://bit.ly/38yaBuk>
15. Qin, P., Wu, K., Hu, Y., Zeng, J., Chai, X.: Diagnosis of benign and malignant thyroid nodules using combined conventional ultrasound and ultrasound elasticity

imaging. *IEEE Journal Of Biomedical And Health Informatics* **9999**(1), 1 (2019). <https://doi.org/10.1109/JBHI.2019.2950994>

- 16. Savardi, M., Benini, S., Signoroni, A.:  $\beta$ -hemolysis detection on cultured blood agar plates by convolutional neural networks. In: International Conference on Medical Image Computing and Computer-Assisted Intervention. pp. 30–38 (2018)
- 17. Schlumberger, M., Tahara, M., Wirth, L.J., Robinson, B., Brose, M.S., Elisei, R., Habra, M.A., Newbold, K., Shah, M.H., Hoff, A.O., et al.: Lenvatinib versus placebo in radioiodine-refractory thyroid cancer. *New England Journal of Medicine* **372**(7), 621–630 (2015)
- 18. Shensa, M.J., et al.: The discrete wavelet transform: wedding the a trous and mallat algorithms. *IEEE Transactions on signal processing* **40**(10), 2464–2482 (1992)
- 19. Simonyan, K., Zisserman, A.: Very deep convolutional networks for large-scale image recognition. *arXiv preprint arXiv:1409.1556* (2014)
- 20. Szegedy, C., Liu, W., Jia, Y., Sermanet, P., Reed, S., Anguelov, D., Erhan, D., Vanhoucke, V., Rabinovich, A.: Going deeper with convolutions. In: Proceedings of the IEEE conference on computer vision and pattern recognition. pp. 1–9 (2015)
- 21. Wang, J., Li, S., Song, W., Qin, H., Zhang, B., Hao, A.: Learning from weakly-labeled clinical data for automatic thyroid nodule classification in ultrasound images. In: 2018 25th IEEE International Conference on Image Processing (ICIP). pp. 3114–3118 (2018)
- 22. Wu, H., Deng, Z., Zhang, B., Liu, Q., Chen, J.: Classifier model based on machine learning algorithms: application to differential diagnosis of suspicious thyroid nodules via sonography. *American Journal of Roentgenology* **207**(4), 859–864 (2016)
- 23. Xie, S., Girshick, R., Dollár, P., Tu, Z., He, K.: Aggregated residual transformations for deep neural networks. In: Proceedings of the IEEE conference on computer vision and pattern recognition. pp. 1492–1500 (2017)
- 24. Xie, Y., Xia, Y., Zhang, J., Feng, D.D., Fulham, M., Cai, W.: Transferable multi-model ensemble for benign-malignant lung nodule classification on chest ct. In: International Conference on Medical Image Computing and Computer-Assisted Intervention. pp. 656–664 (2017)
- 25. Zhang, B., Gao, Y., Zhao, S., Liu, J.: Local derivative pattern versus local binary pattern: face recognition with high-order local pattern descriptor. *IEEE transactions on image processing* **19**(2), 533–544 (2009)
- 26. Zhang, K., Guo, Y., Wang, X., Yuan, J., Ding, Q.: Multiple feature reweight densenet for image classification. *IEEE Access* **7**, 9872–9880 (2019)
- 27. Zhao, J., Zheng, W., Zhang, L., Tian, H.: Segmentation of ultrasound images of thyroid nodule for assisting fine needle aspiration cytology. *Health information science and systems* **1**(1), 5 (2013)
- 28. Zhu, Y., Fu, Z., Fei, J.: An image augmentation method using convolutional network for thyroid nodule classification by transfer learning. In: 2017 3rd IEEE International Conference on Computer and Communications (ICCC). pp. 1819–1823 (2017)